Case Studies in Construction Materials 21 (2024) e04087

Contents lists available at ScienceDirect

Case Studies in Construction Materials

journal homepage: www.elsevier.com/locate/cscm

Microscopic mechanism and predicting calculation on mechanical properties of basalt fiber modified 3D printing cement-based materials

Ben Li [a,*], Kaihang Li [a], Xuetao Lyu [a,*], Canhao Zhao [a], Xianzhang Guan [b]

[a] Advanced and Sustainable Infrastructure Materials Group, School of Civil Engineering and Transportation, Foshan University, Foshan 528000, China

[b] Department of Civil and Environmental Engineering, The Hong Kong Polytechnic University, Hung Hom 999077, Hong Kong

ARTICLE INFO

Keywords:
3D printed cement-based materials
Basalt fibers
Mechanical properties
Multiscale model

ABSTRACT

This study focuses on the modification and intelligent-digital control of 3D printing materials. Based on the significant effect of basalt fiber in improving toughness, the influence mechanism of basalt fiber substitution rate, length and other factors on the macroscopic properties and microstructure scores of 3D printing cement-based materials was explored. The results show that under the combined effect of basalt fiber length and content, the optimal improvement is achieved with 3 % content and 8 mm length, increasing the flexural strength and compressive strength by 10.21 % (28 days) and 13.11 % (28 days), respectively. And the structure has been optimised at the micro level with an increase in type II gels. Also further use of microdata, through data fusion and refined analysis, a model ($R^2 > 0.85$, error < 10 %) and intelligent control method that can comprehensively and accurately predict the service performance of basalt fiber modified 3D printing cement-based materials are established, which provides new development ideas for the intelligent construction and design of future building structures.

1. Introduction

With the development and progress of modern intelligent manufacturing technology, 3D printing cement-based materials are in a stage of vigorous development and become one of the hot research fields (Fig. 1). Compared with the preparation and application of traditional cement-based materials, 3D printing cement-based materials have significant advantages in energy saving, material reduction and cost reduction, and have gradually been recognized and respected [1–13]. The use of 3D printing can save 35–60 % of the cost of building structure, realize the integrated and convenient construction of building materials and structure, and overcome the shortcomings of unstable construction quality and uncontrollable precision [14–18]. However, 3D printing cement-based materials still have problems such as low early mechanical properties, large shrinkage, easy cracking and failure, and weak interlayer bonding properties, which restrict the wide application of related technologies in practical engineering. Therefore, how to effectively improve the service toughness of 3D printed cement-based materials and realize the coordinated development of strength and toughness has become a key issue that needs to be urgently solved in the current research in related fields.

The methods to improve the service toughness of 3D printed cement-based materials mainly include the incorporation of fiber

* Corresponding authors.
E-mail addresses: liben89@fosu.edu.cn (B. Li), lxtwww30@fosu.edu.cn (X. Lyu).

https://doi.org/10.1016/j.cscm.2024.e04087
Received 14 September 2024; Received in revised form 23 November 2024; Accepted 4 December 2024
Available online 4 December 2024

materials (fiber bundles/grids) [19,20], the addition of nanomaterials (nano-silica/nano-titanium dioxide) [21,22] and the change of printing methods (improving equipment accuracy, designing reasonable paths) [23,24]. Among them, improving the mechanical properties of 3D printed cement-based materials by adding fibers is one of the most economical and effective ways. On the one hand, the good adhesion between the fiber and the substrate can reduce the risk of shrinkage damage caused by water loss during the preparation process, thereby ensuring the bonding strength and stability between the layers [25,26]. Tran [27] investigated the effect of PP fiber on the internal friction and bond strength of 3D printed cement-based materials. The results showed that PP fiber could improve the dynamic yield stress and viscosity of the matrix material (increased by 31 % and 94 % respectively when the content was 1.35 kg/m^3). Bohuchval [28] investigated the effect of sisal natural fiber on the permeability and yield stress of 3D printed cement-based materials. The results showed that the sisal natural fiber increased the yield stress of the matrix by 2.8 % and reduced the penetration by 6.7 %. An appropriate amount of fiber can form bridges, filler effects and constraints in the matrix, and bear a certain load, thereby improving the mechanical properties and stability of the material [29,30]. Li [31] analyzed the influence of the incorporation of PVA fiber on the mechanical properties of 3D printed cement-based materials. Their results showed that when the length of PVA fiber was 6 mm and 12 mm, the compressive strength and flexural strength of the matrix reached the highest (41.9 MPa and 10.2 MPa). However, their research results also showed that the mixed incorporation of PVA fiber has a negative impact on the mechanical properties of 3D printed cement-based materials. This is because the mixing of multiple fibers will lead to more serious fiber agglomeration and cannot play a role. Yan [32] showed that the compressive properties of 3D printed ultra-high performance concrete elements can be further improved by using fibre-reinforced polymer wraps. It also evaluates the accuracy of multiple models applied to 3DPC and also shows the depth of predictive models under different conditions.

Although all kinds of fibers have excellent performance in the modification ability of 3D printing cement-based materials, the application of fiber-modified 3D printing cement-based materials in practical engineering is the embodiment of comprehensive interests. The existing research results indicate that the mechanical properties of 3D-printed cementitious materials can be effectively improved by the addition of basalt fibres and show good overall benefits [33,34], both in terms of their yield sources, application costs, and suitability for use with cementitious materials. However, the working performance, volume stability and long-term service performance of the substrate are affected by many factors such as the length, content and type of fiber. In particular, when the basalt fiber content is too large, it is easy to cause the agglomeration of nanomaterials/particles in the matrix, which seriously restricts the modification effect of various properties such as extrusion performance and service performance of 3D printing cement-based materials. Simultaneously, the basalt fiber will change the hydration process of the matrix material, affect the content of hydration products and the distribution of microstructure, and then make the parameter design and macro-micro control of the material become complicated and difficult [35–37]. In contrast, scholars have carried out a certain analysis of the macro-micro correlation of traditional cement-based materials, and used multi-linear, full-quadratic, interactive regression and other models to predict the mechanical properties, and further use the chemical composition data. At the same time, it also shows the contribution of cost perspective, which saves a lot of time for laboratory work [38–40]. Similarly, there is a certain space for the in-depth use of the microscopic data of fiber-modified 3D printing cement-based materials. Therefore, it is necessary to master the influence mechanism of basalt fiber on the macroscopic properties and microstructure of 3D printing cement-based materials, and clarify the decisive factors and key variables, so as to provide theoretical support for the parameter design, performance prediction and effective regulation of fiber-modified 3D printing cement-based materials. At present, the research on the quantitative correlation and influence mechanism between the macroscopic mechanical properties and microstructure of basalt fiber modified 3D printing cement-based materials (BF-3DPC) has just started. Therefore, the goal of this study is to fill these research gaps by investigating the influence of the characteristics of basalt fiber on the macroscopic properties and microstructure of BF-3DPC. At the same time, based on the characteristic analysis and quantitative results of hydration products, the functional relationship between microstructure evolution and macroscopic mechanical properties is proposed. Combining macro-micro experiments and correlation mathematical models, this paper provides theoretical support for the quantitative evaluation and accurate prediction of the mechanical properties of BF-3DPC.

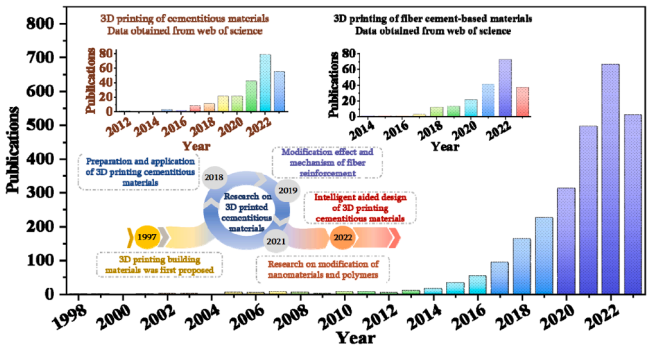

Fig. 1. Statistics of research papers and development on 3D printing cement-based materials.

2. Raw materials and experimental methods

2.1. Raw materials

Cementing material is ordinary Portland cement (P.O 42.5) and its physical properties are shown in Table 1, which conforms to Chinese standard GB 175–2023. Fine aggregate is natural river sand (produced locally) and its physical properties are detailed in Table 2. Chemical constituents of cement and natural river sand are shown in Table 3. The additives include comprehensive polycarboxylic acid water reducing agent (27 % water reduction, 3.0 % gas content, 20 % uric acid ratio) and industrial-grade xanthan gum (in order to print pastes for better setting). The elasticity modulus and tensile strength of basalt fibres are 100 GPa and 3300 MPa. Considering the requirements of practical engineering applications and size influencing factors, the lengths of three basalt fibers were designed to be 6,8, and 10 mm, respectively [41–45].

2.2. Mix proportion design and 3D printing method

Combined with the actual engineering requirements and literature content, the material system in this study was designed as follows [54–59]: 1) The mass ratio of water to cementitious material of basalt fiber modified 3D printing cement-based material (BF-3DPC) is 0.35 and the sand-binder ratio is 1.7. 2) The content of basalt fiber is 2 %, 3 % and 4 % mass ratio of cementitious materials. 3) The content of polycarboxylate superplasticizer and Xanthan gum is 0.2 % and 1.7 % mass ratio of cementitious material. Xanthan gum is used as a thickener to improve and enhance the stability of the printing matrix. According to the corresponding design details and concepts, the specific coordination of basalt modified 3D printing cement-based materials is shown in Table 4. In addition, it should be noted that unlike the traditional mixing process of cement-based materials, the preparation process of 3D printing additive manufacturing cement-based materials is a key step that requires more significant detailed thinking and design. The preparation process of basalt fiber modified 3D printing cement-based material is shown in Fig. 2. Firstly, the cementitious material is mixed with the aggregate for 120 seconds and then the basalt fiber is added to mix for 90 seconds. Subsequently, water, water-reducing agent and xanthan gum were added and mixed for 120 seconds to make all kinds of materials mixed evenly. In the early stage of preparation, the extrusion rate and nozzle diameter of the 3D printer were set to a fixed value (4000 mm/min and 40 mm). In the printing process, the printing path of each layer of substrate was designed to be following zigzag mode, and stacked after the previous layer was printed. Finally, the specimens with sizes of 40 × 40 × 160 mm and 100 × 100 × 100 mm were prepared. All specimens were treated with standard curing until 7 days, 14 days and 28 days (20 ± 2°C, RH≥95 %).

2.3. Experimental method and design

2.3.1. Macroscopic physical properties of BF-3DPC

The experimental test methods of flow properties and mechanical properties of basalt fiber modified 3D printing cement-based material were carried out with reference to GB/T 2419-2005 and GB/T 17671-1999, respectively. The equipment used is HYZ-300-10 type press-folding integrated machine. The loading speed of flexural test is 50 N/s ± 10 N/s and the loading speed of compressive test is 2400 N/s ± 200 N/s [60,61].

2.3.2. Characterization of microstructure evolution in BF-3DPC

The Ca elemental composition and variation of basalt fiber modified 3D printing cement-based material were detected by XPS (Axis-ultradld instrument). At the same time, the functional group changes of BF-3DPC matrix material were characterized by FTIR detection (FTIR-960 Fourier transform infrared spectrometer). Changes of micro-area structure and morphology of BF-3DPC was qualitatively analyzed based on SEM method (GeminiSEM 300 scanning electron microscope). In addition, in order to provide quantitative and accurate microscopic composition data for theoretical calculation and analysis, the chemical composition of BF-3DPC was analyzed by Q-XRD method. In the process of Q-XRD semi-quantitative analysis, corundum (Al_2O_3) was used as the internal standard reference, and the relative phase content was tested by the internal standard method. The phase retrieval identification and quantitative calculation of phase relative content were carried out by using JADE software and the PDF-4 2018 database of the International Diffraction Data Center (ICDD). Among them, the phase quantitative analysis uses the reference strength ratio (RIR method) to calculate the mineral mass fraction [62–67].

Table 1
Physical and mechanical properties of cement [46–48].

3 Days Flexural strength (MPa)	28 Days	3 Days Compressive strength (MPa)	28 Days	Fineness (m^2/kg)	Initial setting Setting time (min)	Final setting
4.2	8.5	23.5	43.2	331	186	252

Note: The fineness of these is expressed using the sieve residue method.

Table 2
Main physical properties of fine aggregates [49–53].

River sand	Particle size (mm)	Surface density (kg/m^3)	Stack density (kg/m^3)	Fineness modulus	Water absorption (%)	PH
	≤ 2.6	2650	1640	2.6	17.5	6.48

Table 3
Chemical properties of cement and sand (%).

Materials	Chemical Compositions (%)						
Cement	SiO_2	CaO	Al_2O_3	Fe_2O_3	MgO	SO_3	LOI
	21.47	60.93	5.80	4.04	3.24	2.08	2.44
River sand	SiO_2	LOI					
	99.88	0.12					

Note: The LOI is the loss on ignition of material.

Table 4
Mix design of basalt fiber modified 3D printing cement-based material.

Number	Water (kg/m^3)	Cement (kg/m^3)	River Sand(kg/m^3)	Water reducer (%)	Xanthan gum (%)	Fiber content (%)	Lengths (mm)
BF00	262.5	750	1275	0.2	1.7	0	0
BF26	262.5	750	1275	0.2	1.7	2	6
BF36	262.5	750	1275	0.2	1.7	3	6
BF46	262.5	750	1275	0.2	1.7	4	6
BF28	262.5	750	1275	0.2	1.7	2	8
BF38	262.5	750	1275	0.2	1.7	3	8
BF48	262.5	750	1275	0.2	1.7	4	8
BF210	262.5	750	1275	0.2	1.7	2	10
BF310	262.5	750	1275	0.2	1.7	3	10
BF410	262.5	750	1275	0.2	1.7	4	10

Note: 1) BF in BF410 denotes basalt fiber. 2) 4 denotes fiber doping. 3) 10 denotes fiber length.

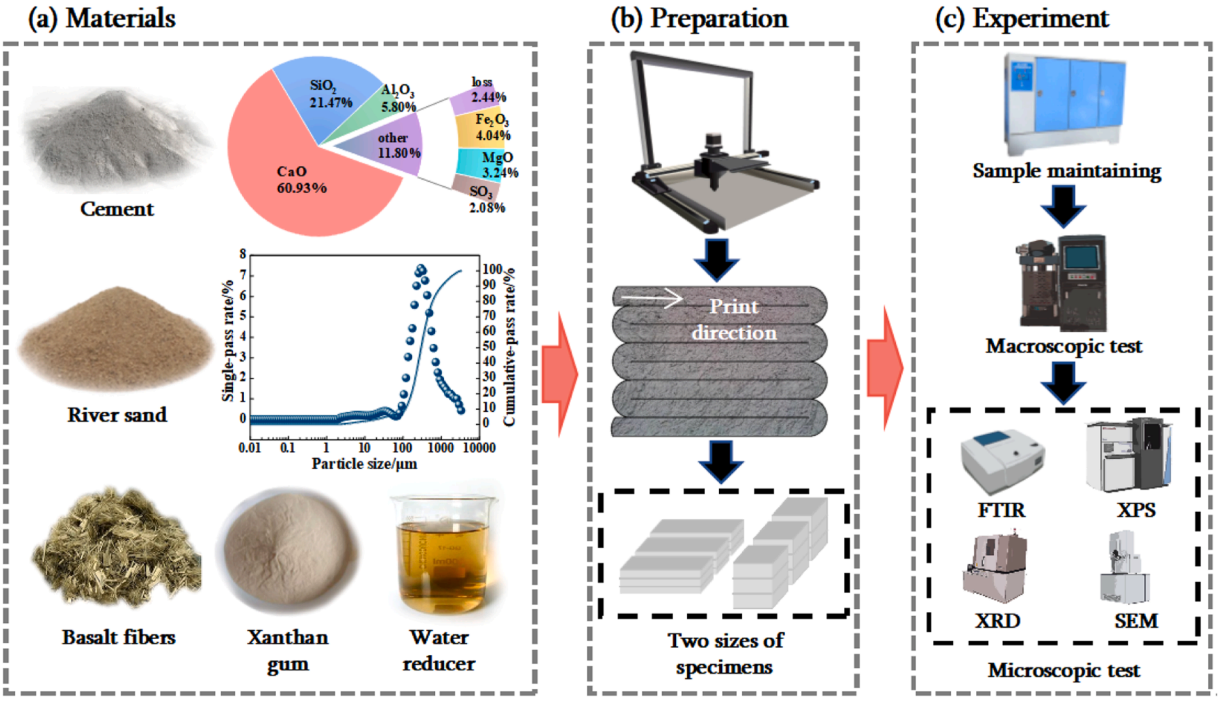

Fig. 2. The specimen preparation process of basalt modified 3D printing cement-based materials.

3. Results and discussion

3.1. The fluidity and mechanical properties of BF-3DPC

The fluidity properties of BF-3DPC based on the influence of content and length of basalt fiber is shown in Fig. 3(a). It can be found that basalt fiber has a significant adverse effect on the flow properties of 3D printed cement-based materials. A single increase in the length of the fibers or in the amount of fibers doped can cause a decrease in flowability. The increase of basalt fiber content leads to agglomeration and adhesion of more mortar, which aggravates the flow obstruction inside the matrix and causes uneven dispersion of free water. The flow performance of BF26 was close to that of the reference group (only decreased by 2.71 %). This compares to a 7.69 % decrease in BF46. However, when the content was 4 % and the length was 10 mm, the flow performance of BF410 was the worst (18.6 % lower than that of the reference group). This is due to the fact that the increase in basalt fiber length creates a spatial lattice structure, which further reduces the flow properties of the 3D printing matrix. However, when the two factors work together, the hindering effect becomes complicated and amplified, and thus a significant decrease in the flow properties of BF-3DPC occurs. Although factors such as fiber content and length have a negative effect on the flow performance, the prepared material is still in a good plasticity range and can meet the needs of 3D printing. Compared with the negative effect of basalt fiber on the flow performance, it has a significant mechanical strengthening effect on 3D printed cement-based materials. When the length of basalt fiber does not exceed 10 mm, the compressive strength and flexural strength of 3D printed cement-based materials increase first and then decrease with the increase of fiber content (Fig. 3(b) and (c)). The BF38 group with a fiber content of 3 % and a length of 8 mm had the most compressive strength and flexural strength, which were 19.22 % (7d), 19.56 % (7d) and 10.21 % (28d), 13.11 % (28d) higher than BF00. The application of appropriate basalt fibers can better utilize their bridging and tensile properties to enhance the mechanical properties. The mechanical properties of 3D printed cement-based materials show a continuous decrease with the increase of fiber content when the length of basalt fiber is 10 mm. The compressive and flexural strengths of BF410 were 13.7 % and 15.9 % (7d), 17.3 % and 10.3 % (28d) lower than those of BF00. When the fiber length and the amount of too large not only affect the fluidity, the agglomeration effect will be prone to produce internal defects and can not play a good fiber itself excellent performance. The early mechanical properties of BF-3DPC are most directly affected by the change of fiber length, and the mechanical properties at standard age are related to the coupling effect of fiber length and dosage.

The engineering pouring of traditional cement-based materials is carried out by vibrating the mixture during the pouring process to eliminate bubbles and ensure the compactness and uniformity of the concrete. In contrast, the nozzles of 3D printing cement-based materials are printed layer by layer and stacked layer by layer, and there will be some defects such as interlayer voids, weak transition surfaces and bubbles, which will affect the overall mechanical properties. The incorporation of basalt fiber can form a composite stable network space structure inside the matrix, thereby improving the early strength and toughness of the matrix and hindering the

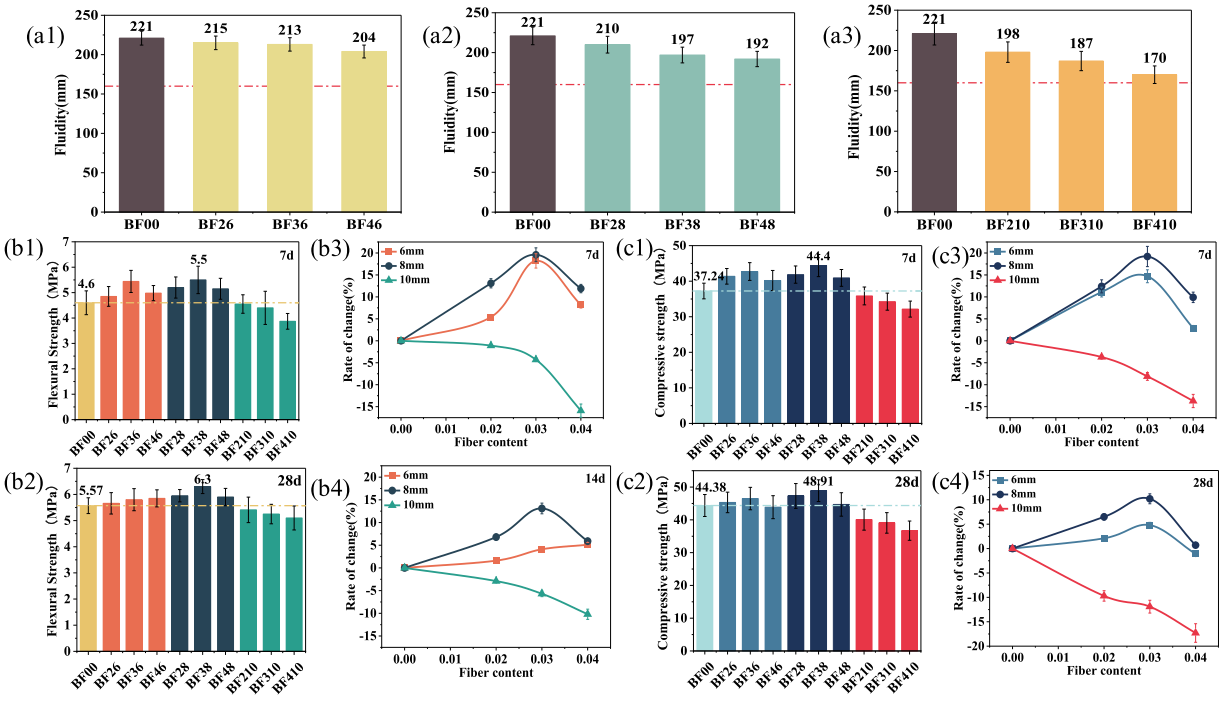

Fig. 3. Macroscopic performance of BF-3DPC. (a) The changes of fluidity performance. (b) Flexural strength and relative change rate. (c) Compressive strength and relative change rate.

further development of cracks. Therefore, the incorporation of fibers within a certain length range can better improve the early mechanical properties of 3D printed cement-based materials. However, when the fiber length exceeds a certain value, too long basalt fiber will disturb the interlayer stability of the matrix material, hinder the hydration hardening process and expand the interlayer disadvantage, and eventually lead to insufficient modification of mechanical properties.

3.2. The evolution law of microstructure in BF-3DPC

Various microscopic analysis methods were used to explore the evolution patterns of functional groups (FTIR), chemical binding energy (XPS), hydration products (Q-XRD) and microstructure characteristics (SEM) of BF-3DPC. This research combined macroscopic experimental data and analysis results and selected BF00, BF28, BF38 as the experimental groups. At the same time, this research considers the preparation process and spatial distribution of 3D printed cement-based materials, mainly focusing on fine, multi-point, and multi type sampling work between layers and inside the substrate. Finally, the obtained samples were immersed in an alcohol solution and sealed to prevent the influence of re-hydration of the sample on the microscopic analysis results.

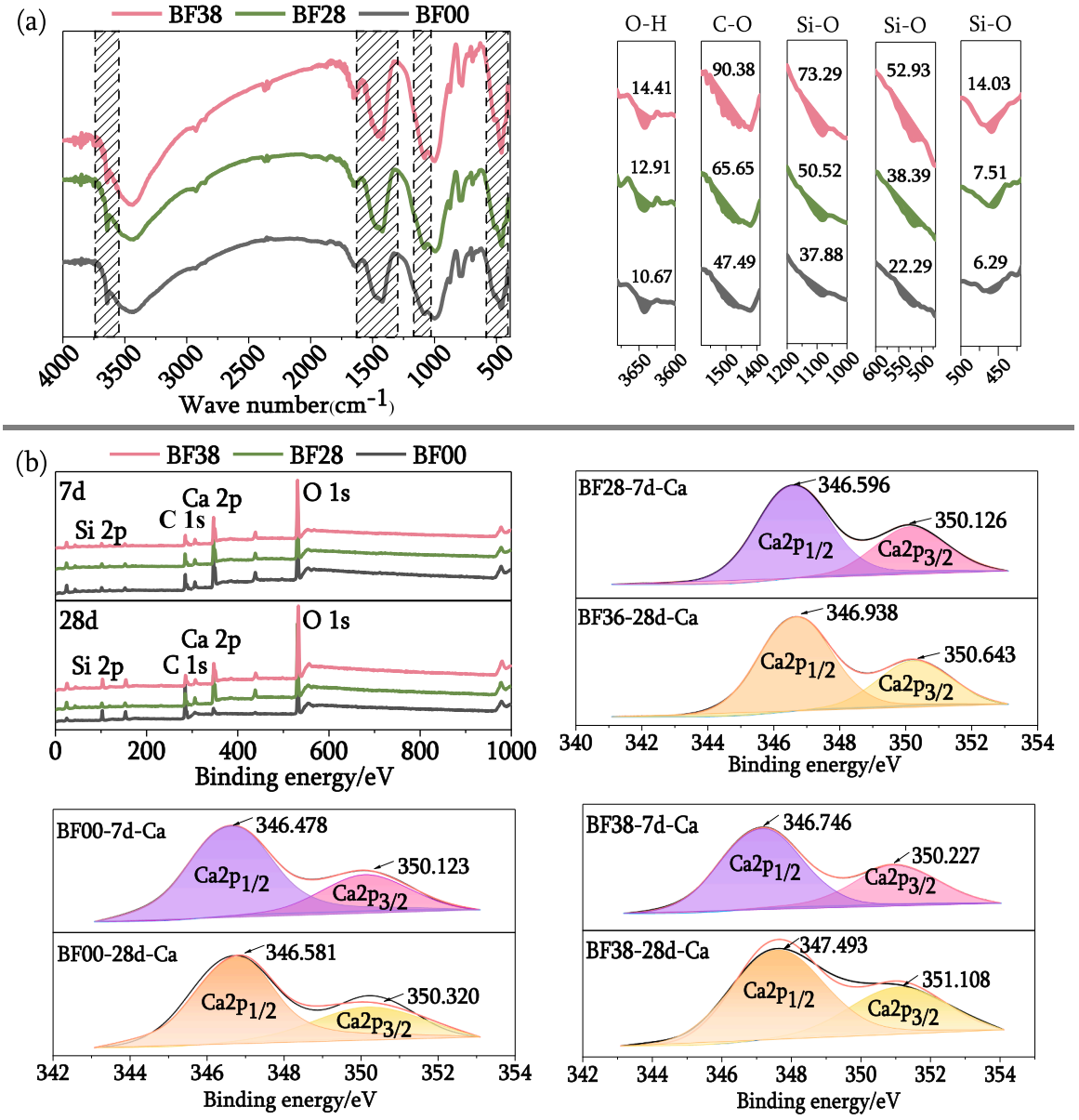

Fig. 4. (a) Changes in chemical functional groups. (b) Chemical binding energy and deconvolution calculation results on calcium ion.

3.2.1. Evolution of functional groups and chemical binding energy of BF-3DPC

The variation of functional groups of BF-3DPC during 28 days is shown in Fig. 4(a). The results show that basalt fibers with different contents and lengths will not change the types of key chemical bonds in the matrix material, but will change the distribution of functional groups. With the increase of basalt content, the O-H bond in CH (3640 cm^{-1}) and the C-O bond stretching vibration peak in $CaCO_3$ (1426 cm^{-1}) have undergone to a limited extent vibration. The incorporation of basalt fiber will partially consume CH and lead to the further formation of $CaCO_3$. It is worth noting that Si-O tensile absorption peak (1090 cm^{-1}), Si-O outward bending vibration absorption peak (525 cm^{-1}) and Si-O inward bending vibration absorption peak (455 cm^{-1}) in C-S-H also change with the increase of basalt fiber content. The incorporation of basalt fiber can promote the formation of the main hydration product C-S-H gel in the substrate, especially the conversion of CH to C-S-H (II) gel.

Based on quantitatively analyzing the evolution on chemical binding energy of matrix material and binding energy of calcium ions in C-S-H, the influence of basalt fiber on the chemical structure of 3D printed cement-based materials was further discussed. On one hand, the chemical binding energy and O, Ca, C, and Si elemental peaks of BF00, BF28 and BF38 at 7 and 28 days of standard curing were shown in Fig. 4(b). Under the coupling effect of curing age and basalt fiber content, the binding energy of Ca^{2+} in the hydration product C-S-H gel of 3D printing substrate gradually increased. For example, the binding energy peak of BF38 at 28 curing days has a certain right shift compared with BF00. In addition, according to the energy peak position of calcium element, it is divided into $Ca2p_{1/2}$ and $Ca2p_{3/2}$. The binding energy of $Ca2p_{1/2}$ and $Ca2p_{3/2}$ in the C-S-H hydration products of BF38 was higher than that of BF00, which increased by 0.104–0.268 (7d), and 0.74–0.78 (28d), respectively. This is because an appropriate amount of basalt fiber can promote 3D printed cement-based materials in a rich conditions of calcium ions, which can increase the orbital binding energy of calcium ions and promotes the formation of more calcium and gel phases, thereby contributing to the nucleation and crystal growth of hydration products.

3.2.2. Changes in microstructure and hydration products of BF-3DPC

The microstructure of BF-3DPC is shown in Fig. 5(a)-(b), it can be seen that the application of basalt fiber has a certain optimization effect on the microstructure of 3D printing cement-based materials. In the early curing stage, BF00 has obvious pore cavity defects and structural evacuation, while BF38 has fewer defects and relatively dense structure. Basalt fiber can play a better filling role and

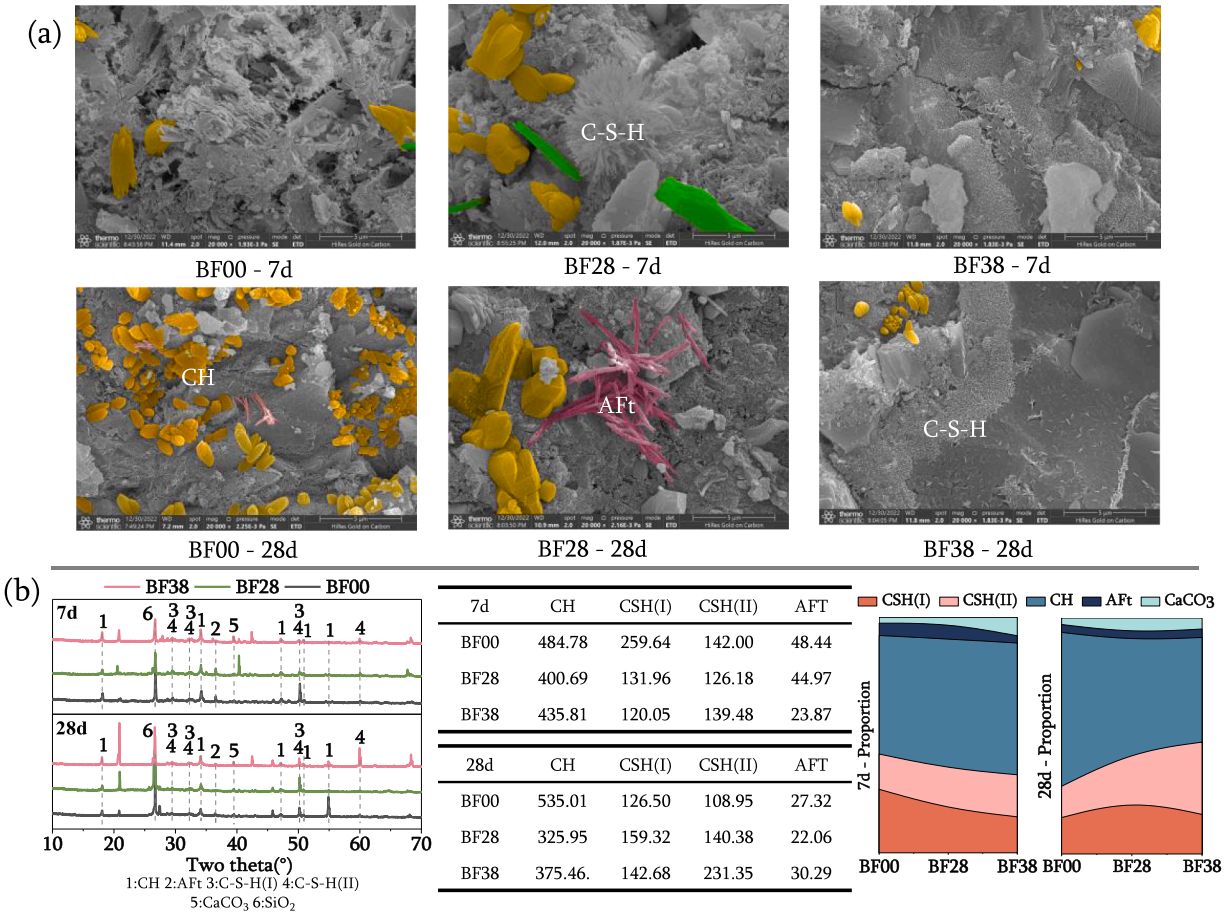

7d	CH	CSH(I)	CSH(II)	AFT
BF00	484.78	259.64	142.00	48.44
BF28	400.69	131.96	126.18	44.97
BF38	435.81	120.05	139.48	23.87

28d	CH	CSH(I)	CSH(II)	AFT
BF00	535.01	126.50	108.95	27.32
BF28	325.95	159.32	140.38	22.06
BF38	375.46.	142.68	231.35	30.29

Fig. 5. (a) Microstructure and morphology analysis. (b) Changes in the type and relative phase content of hydration products.

optimize the compactness of hydration products, thereby improving the microstructure of BF-3DPCD (initial age). With the progress of curing, the influence of basalt fiber on the microstructure of 3D printed cement-based materials is more significant. The appropriate amount of basalt fiber has good compatibility with the matrix material, which can play a synergistic role and improve the compactness of the matrix material and repair micro-cracks by bridging and filling. It is worth noting that an appropriate amount of basalt fiber can affect the formation of C-S-H gel and hydration products such as CH, promote the formation of a denser microstructure, and improve the macroscopic properties and material structure of BF-3DPC to a certain extent. In addition, the incorporation of basalt can also affect the microstructure between the matrix and the matrix. An appropriate amount of basalt fiber can promote the transformation of CH to high-density C-S-H gel, thereby weakening the effect of CH on interlayer stability and defect distribution. The relative phase contents of C-S-H (I) and C-S-H (II) in BF38 were increased by 12.79 % and 123.53 % (28 d) compared with BF00. Combined with the changes of CH in various microscopic experiments, an appropriate amount of basalt fiber incorporation has a very positive effect and positive effect on the consumption of CH to generate high-density C-S-H (II) type gel, which is also the key to improving the macroscopic properties of 3D printed cement-based materials.

3.3. Parametric model and mechanical properties prediction of BF-3DPC

Basalt fiber, when used appropriately, can significantly enhance the macroscopic properties and microstructure of BF-3DPC, particularly improving its toughness and inter-laminar shear resistance. However, optimizing the design and control of service performance for different composition systems and ratio requirements, as well as accurately predicting and effectively managing the practical application and service characteristics of BF-3DPC, remain challenging in current research. Therefore, the key to addressing these difficulties lies in clarifying the quantitative relationship between basalt fiber parameters and the microstructure of BF-3DPC and establishing a macroscopic mechanical evolution model based on microstructural changes. This paper presents a mathematical model for characterizing the mechanical properties of BF-3DPC based on microstructural variations (Fig. 6). The computational approach and analytical principles are as follows: 1) Summarizing and categorizing multi-scale parameters based on physical principles, and processing relevant parameter datasets quantitatively to obtain initial data. 2) Using the compiled dataset as input for regression analysis to establish functional equations between basalt fiber parameters and hydration product content. The accuracy of these equations is assessed using correlation coefficients, and the rationality and effectiveness of the mathematical equations are further optimized by adjusting the weights and sensitivities of relevant parameters. 3) Based on the quantitative equation for hydration products, proposing correlation equations between hydration products and macroscopic mechanical properties, and calculating the variation patterns of compressive and flexural strengths of BF-3DPC. The computed mechanical property results are compared with experimental data to verify the validity and accuracy of the regression calculations. Subsequently, adjustments to the main algorithm parameters are made promptly by analyzing the causes of calculation errors.

3.3.1. Preparation and preprocessing of data sets

The accuracy of regression calculations depends heavily on data selection and quality. Therefore, it's crucial to preprocess and carefully choose the raw data before conducting calculations and analyses [68–70]. In this study, various parameters of BF-3DPC undergo preprocessing steps prior to mathematical analysis: 1) Key input variables such as curing age, water-cement ratio, sand-cement ratio, water reducing agent, fiber length, and fiber content are defined. These variables are organized into datasets using

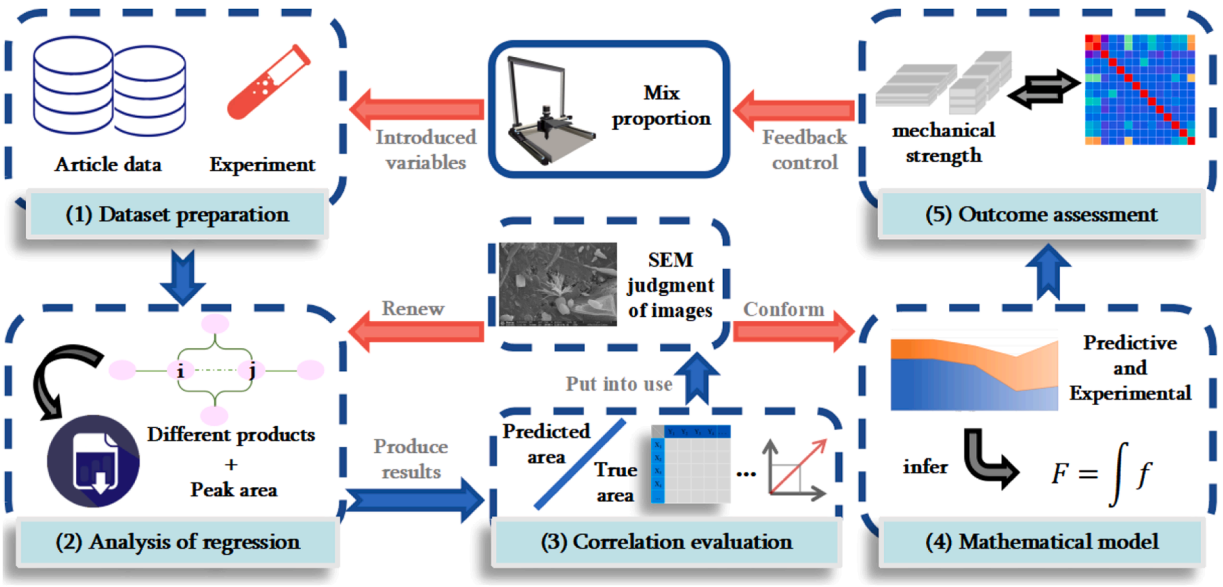

Fig. 6. Quantitative research process of macroscopic mechanical properties and microstructure of BF-3DPC.

feature selection and dimensionless methods. 2) Similarly, the relative phase content (Q-XRD) of critical hydration products, the envelope area (XPS) of chemical element binding energies, and the compressive and flexural strengths serve as output results. These outputs are then organized into dimensionless datasets.

3.3.2. *Calculation results on microstructure evolution of BF-3DPC*

Considering the coupling influence of the length, parameters and ratio design of basalt fiber on the relative phase content and chemical binding energy of hydration production, a two-layer hidden layer artificial neural network model is used to establish the mathematical characterization and prediction analysis on the microstructure evolution law as follows:

$$\Theta_{hy} = \sum_{n=1}^{n=n} [W_1 X_1 + \cdots + W_n X_n] + \sum_{n=1}^{n=n} [b_1 + \cdots + b_n] \tag{1}$$

$$\Theta_{co} = \sum_{n=1}^{n=n} [W'_1 X_1 + \cdots + W'_n X_n] + \sum_{n=1}^{n=n} [b'_1 + \cdots + b'_n] \tag{2}$$

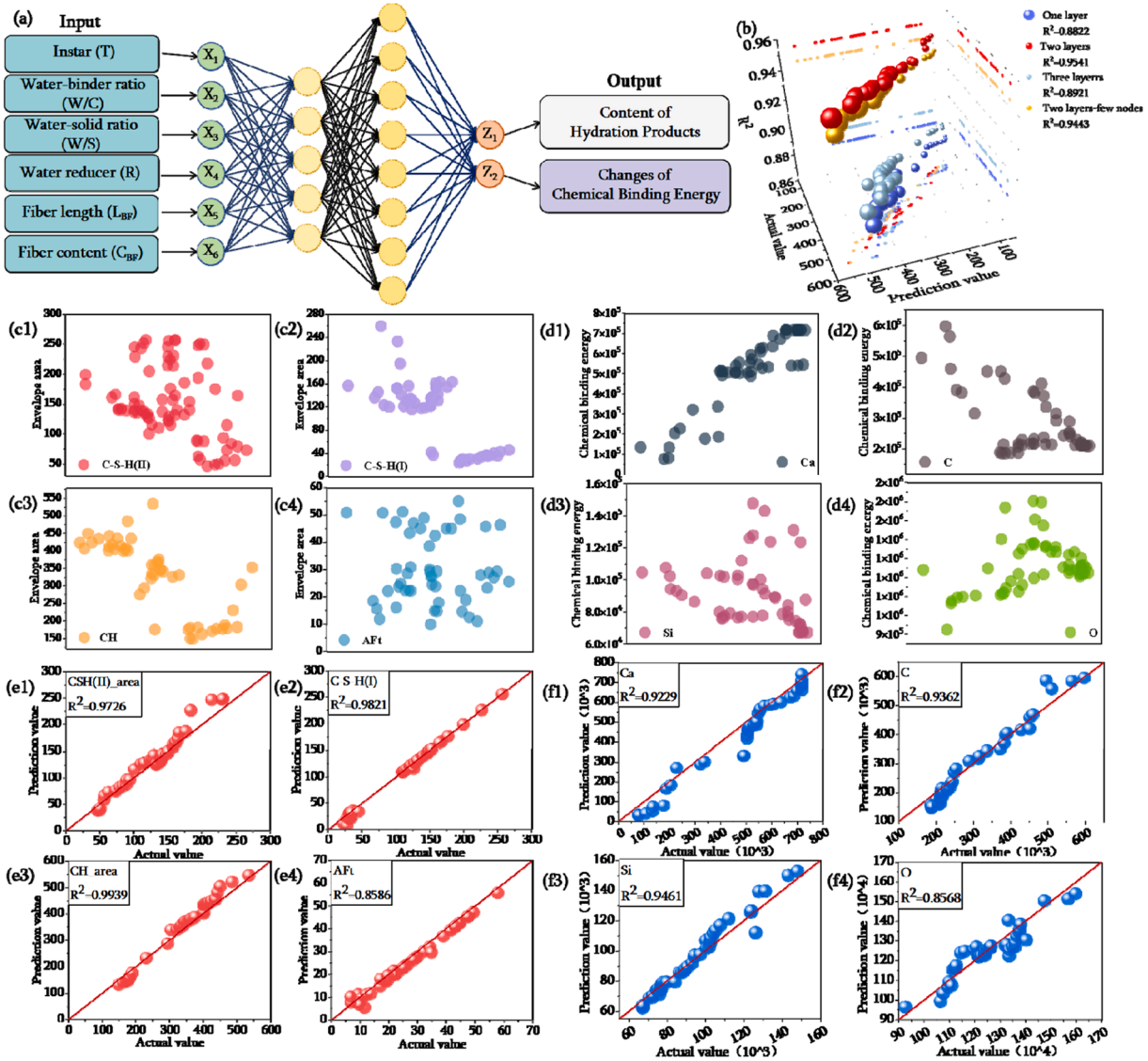

Fig. 7. The calculation results on relative phase content and chemical binding energy of BF-3DPC. (a) Main parameters and calculation process. (b) Accuracy analysis of different calculation models. (c) Calculation results of main hydration products content. (d) Calculation results of chemical binding energy of main elements. (e) The correlation analysis between the calculated value and experimental results of hydration product content. (f) The correlation analysis between the calculated value and experimental results of chemical binding energy.

where, $\Theta_{hy}$is the relative phase content, $\Theta_{co}$is the chemical binding energy, $W$and $W'$is the weight index of influencing factors,$X$is the macroscopic influencing factors, b and b′ is the correction parameter.

The analysis results on the envelope area changes in phase content of the main hydration products such as C-S-H (I), C-S-H (II), CH and AFt are shown in Fig. 7(c). The results show that the envelope area distribution of C-S-H (I), C-S-H (II), CH, the three main hydration product phases has a certain concentration area and is dispersed in a certain interval. The envelope area distribution of the phase content of AFt is more random and dispersed. The analysis results on the envelope area changes in Chemical binding energy such as C, Ca, O and Si are shown in Fig. 7(d). The distribution of the chemical binding energy envelope area results of the four elements of Ca, C, Si and O also shows a certain concentration, but it is affected by the increase of the distribution span, and some discrete points appear in the results. Then the correlation between the predicted value and the real value is analyzed and compared, and the results are shown in Fig. 7(e)-(f). It can be seen that due to the influence of the data point concentration area, the calculation results of the C-S-H gel phase envelope area show a high correlation with the real value (R^2 is preferably 0.9821), which is 12.57 % higher than the prediction correlation of AFt with more dispersed data points. On the other hand, the existence of some discrete points will have a negative impact on the accuracy of the calculation. It can be seen that the correlation of the overall chemical binding energy calculation results is slightly lower than that of the relative phase content calculation results. However, whether it is the calculation of relative phase content or chemical binding energy, R^2 can reach more than 0.85, indicating that this model has certain applicability to the calculation of microstructure evolution.

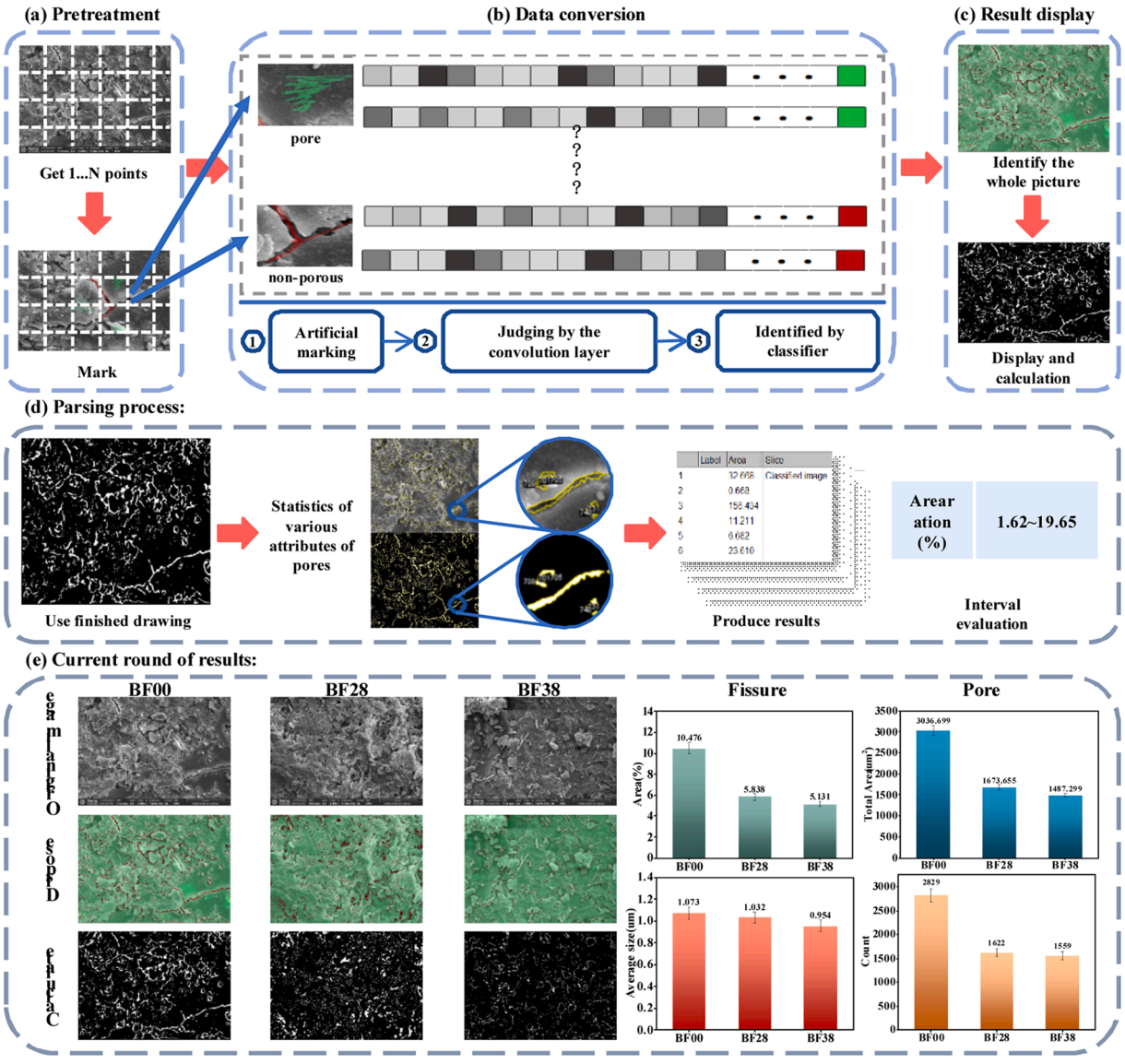

Fig. 8. Discriminant basis and calculation process on microstructure evolution of BE-3DPC.

3.4. Discriminant basis for the calculation on microstructure evolution

It is feasible to calculate the microstructure evolution of BF-3DPC through the two-layer hidden layer model and has a certain accurate feedback ability. However, due to the complex evolution of the microstructure, the calculation data set will be too large and the calculation process will be lengthy, which will affect the accuracy and simplicity of the calculation and analysis. Meanwhile, the multi-scale and cross-scale effects and the error of experimental characterization may produce the error of microstructure information and the deviation of calculation results in the process of data calculation and analysis with high accuracy requirements. In addition, in the process of judging the accuracy and authenticity of the calculation results, it is necessary to add additional judgment basis to realize the accurate evaluation of the authenticity and validity of the calculation results. Therefore, based on the quantitative results of image recognition, this study proposes the judgment conditions of BF-3DPC microstructure evolution calculation, which serves to improve the accuracy and effectiveness of the calculation structure [71]. The microstructure image of BF-3DPC is meshed and the crack and pore structure are marked in the mesh. Meanwhile, the image recognition calculation software is used to identify and analyze the micro-cracks and pore structures in each region in detail and form a classifier of relevant image data. The recognition analysis and calculation of the global area of the image are carried out by the classifier, focusing on the calculation of the size and area of the crack and pore structure. Finally, based on the area ratio of microstructure such as crack and pore structure, the area ratio range is set as the criterion to feedback the compactness of BF-3DPC microstructure and verify the accuracy of the calculation results. The identification and calculation results on proportion of crack area, average crack size, total area and number of pore in BF00, BF28 and BF38 is 10.476–5.131 %, 1.073–0.954 μm, 3036.699–1487.299 μm^2 and 2829–1559, which is the determination range of the select ability and rationality of microstructure data in BF-3DPC. The flow of this block is presented in Fig. 8.

3.4.1. Mechanical prediction model based on quantitative results of microstructure evolution of BF-3DPC

The macroscopic mechanical properties of BF-3DPC are closely related to the evolution of microstructure, and the change of microstructure is affected by content or length of BF, water-cement ratio and other factors. Based on the quantitative research results of microstructure and the criterion conditions of calculation, a theoretical model for calculating and predicting the mechanical properties of BF-3DPC was established. Considering the factors such as curing age and hydration products, the response indexes of various factors to the mechanical properties of BF-3DPC were proposed as:

$$M = \frac{\widehat{\Theta}_{hy,28}}{\Theta_{hy,28}} \cdot \left(\widehat{\Theta}_{hy,28} - \widehat{\Theta}_{hy,7} \right) \tag{3}$$

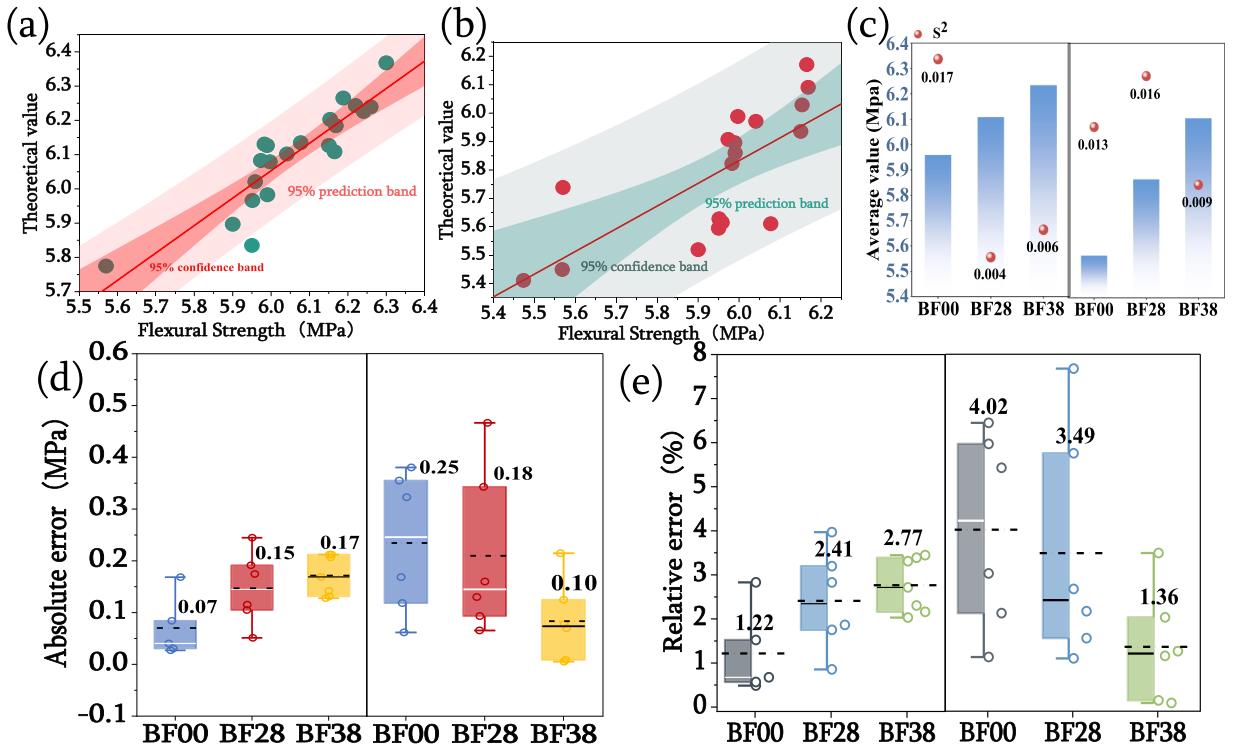

Fig. 9. The calculation results of flexural strength. (a) Based on changes in hydration products. (b) Based on changes of chemical binding energy. (c) Calculated mean and variance. (d) The error between calculation and experiment. (e) The error ratio between calculation and experiment.

$$M_D = \sum |M[C-S-H(I)] + M[C-S-H(II)] + M[CH] + M[AFt] + \cdots| \tag{4}$$

$$M' = \mathfrak{F}^{Si}_{co,7} \cdot \frac{\Theta_{co,28} - \Theta_{co,7}}{\Theta_{co,28}} \tag{5}$$

$$M_S = \sum |M'[Si] + M'[Ca] + M'[C] + M'[O] + M'[H] + \cdots| \tag{6}$$

where, M is the influence parameters of hydration content, M' is the influence parameters of chemical binding energy, M_D is the comprehensive response indicators of hydration content, M_S is the comprehensive response indicators of chemical binding energy, $\Theta_{hy,28}$ is the total relative phase content of hydration product at 28 day, $\widehat{\Theta}_{hy,28}$ is the characteristic peak on relative phase content of hydration product at 28 day, $\widehat{\Theta}_{hy,7}$ is the characteristic peak result on relative phase content of hydration product at 7 day, $\Theta_{co,7}$ and $\Theta_{co,28}$ are the chemical binding energy of main element at 7 and 28 day, $\mathfrak{F}^{Si}_{co,7}$ is the parameters for promoting hydration process by combining with silicon at early curing time.

According to the changes of hydration products and micro structure, the calculation model of compressive and flexural strength of BF-3DPC is deduced as follows:

$$F_f(M_D) = 0.16 \cdot \widehat{\Theta}^{\mathrm{C-S-H(II)}}_{hy,7} + [\ln(M_D)]^2 \quad F_f(M_S) = 0.14 \cdot \ln\left(\Theta^{Si}_{co,7}\right) + \ln\left((M_S)^3\right) \tag{7}$$

$$F_c(M_D) = 1.3 \cdot \widehat{\Theta}^{\mathrm{C-S-H(II)}}_{hy,7} + [\ln(M_D)]^2 \quad F_c(M_S) = 1.08 \cdot \ln\left(\Theta^{Si}_{co,7}\right) + \ln\left((M_S)^3\right) \tag{8}$$

where, $F_f(M_D)$ and $F_c(M_D)$ are the calculation results of flexural and compressive strength based on hydration products, $F_f(M_S)$ and $F_c(M_S)$ are the calculation results of flexural and compressive strength based on chemical binding energy, $\widehat{\Theta}^{\mathrm{C-S-H(II)}}_{hy,7}$ and $\Theta^{Si}_{co,7}$ are the characteristic peak of relative phase content of C-S-H (II) and the chemical binding energy of silicon at 7 day.

The calculated results on flexural strength and compressive strength of BF-3DPC are shown in Figs. 9 and 10. The maximum calculation error value of flexural and compressive strength obtained based on hydration products is 0.24 MPa and 0.65 MPa (Mean values range from 0.07 to 0.17 and from 0.29 to 0.38.), and the maximum calculation error rate is 3.96 % and 1.40 % (Mean values range from 1.22 to 2.77 and from 0.58 to 0.84.), respectively. However, the calculation results of mechanical properties using chemical

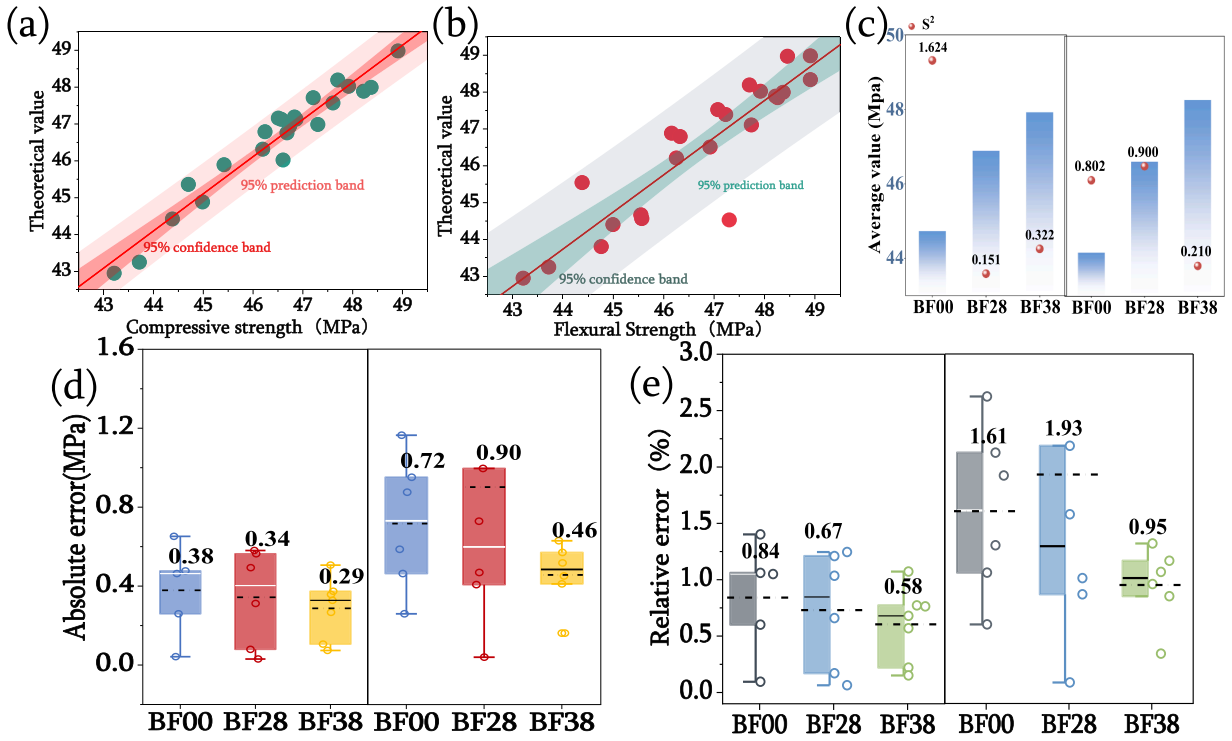

Fig. 10. The calculation results of compressive strength. (a) Based on changes in hydration products. (b) Based on changes of chemical binding energy. (c)Calculated mean and variance. (d) The error between calculation and experiment. (e) The error ratio between calculation and experiment.

binding energy have relatively large error values and error rates (0.46 MPa (7.67 %) and 2.76 MPa (5.85 %)). From Figs. 9c and 10c it can be seen that using chemical binding energy calculations reduces the dispersion of the data without fibre groups, but causes dispersion with fibres. Although the mechanical strength development law of BF-3DPC can be calculated based on the chemical binding energy, it cannot feedback the influence of interlayer bonding and overall hardening of the material during the calculation process, resulting in a certain deviation in the calculation results. Especially in the calculation of bending and flexural toughness, based on the evolution of hydration products can get better calculation results. In order to obtain more accurate calculation and prediction results to achieve the purpose of reverse design of materials, it is still necessary to optimize the data acquisition and calculation process. On the one hand, through the representative sampling and microscopic experimental analysis of multi-directional and multi-regional space, a systematic microstructure evolution data set is formed. On the other hand, it is necessary to consider the deformation synergistic response between the material layer and the whole under load, and improve the accuracy of calculation from the perspective of material-structure-mechanics.

3.5. Intelligent applications and practical engineering prospects of BF-3DPC

Compared with traditional cement-based materials, basalt fiber modified 3D printing cement-based materials show flexible construction, can realize rapid prototyping of complex structures, and reduce material waste and construction time. But in its in-depth application, based on the previous research and model derivation, considering the complexity of parameters and computational challenges in 3D printing composites, the use of microstructures in multiple directions has advantages in promoting model calculation. Despite the model being subject to errors, continuous enrichment and optimization are achievable by incorporating data from existing or future research data and actual engineering indicators. This approach offers practical guidance for the preparation of 3D printed cement-based materials. The introduction of model analysis for the application of 3D printing materials not only reduces the test cost of matrix materials, improves the test efficiency, but also ensures the consistency in the construction process of 3D printing buildings (Fig. 11). Looking ahead, diverse building styles can be designed to correspond with actual applications, allowing designers to predict and control real-time performance through intelligent Platforms. This enables more rapid implementation of precise calculations in matrix formulation for structure printing. Such research endeavors contribute to steering the basalt fiber reinforcement system towards a more modern and controllable direction.

Although we put forward this idea, considering the complexity of construction and service conditions in practical engineering, and due to the limitation of existing data, it has not played a broad representative role in the ion dormitory, long-term mechanics, freeze-thaw and other effects of basalt fiber 3D printing cement-based materials. Therefore, it is still necessary to enrich the research on the long-term performance mechanics and durability of basalt 3D printed cement-based materials in extreme service environments, and expand data resources.

4. Conclusions

In this manuscript, the fluidity, mechanical properties and microstructure of basalt fiber reinforced 3D printing cement-based materials were studied and analyzed. The evolution equation of hydration product phase content and chemical binding energy was proposed, and the relationship between microstructure evolution and macroscopic mechanical properties of basalt fiber modified 3D printing cement mortar was explored, which provided some help for the popularization and application of basalt fiber 3D printing cement-based materials. The main conclusions are as follows:

(1) When basalt fibers are doped, the increase of their length and dosage decreases the flow performance of 3D printed cement-based materials. However, when the fiber doping is in the range of 0–4 % mass ratio and the fiber length is 6–10 mm, the flow properties of the printed slurry can meet the requirements.
(2) The basalt fiber content of 0–3 % mass ratio has a reinforcing effect on the mechanical properties of 3D printed cement-based materials. The optimum dosage is 3 %, the length is 8 mm, the flexural strength is 6.3 MPa, and the compressive strength is 48.91 MPa.
(3) The incorporation of basalt fiber is helpful to the interlayer hydration of 3D printing cement-based materials. In the interlayer hydration of C-S-H cementitious phase, the incorporation of fiber increases the hydration formation ratio of C-S-H cementitious phase and reduces the dispersion of crystalline by-products. Among them, the 3 % content has the best promotion effect, but when the fiber content is greater than 3 %, the interlayer defects expand.
(4) By predicting the R^2 value of the product content and binding energy by the prediction model, it can be seen that the model has certain availability (R^2 >0.85). At the same time, by comparing the two, it can be found that the prediction of hydration products by using the external mixing variables as input values has better results. After that, the correlation equation also shows the same advantage for the mechanical calculation results (error<10 %). This also shows that the correlation model can better predict the microstructure evolution and mechanical properties of 3D printed cement-based materials, and provide new ideas for the evaluation of the mechanical properties of 3D printed cement-based materials.

5. The challenges and limitations that arise

Despite the ideas expressed above, due to the complexity of construction and use conditions in actual engineering, as well as the limitations of existing data, the effects of harmful ion erosion, long-term mechanics, freeze-thaw and other factors on the properties of

Fig. 11. Technology prospect of digital assisted BF-3DPC [72–75]. The top left picture is from: https://www.dw.com/en/is-3d-printing-the-future-for-building-homes/a-58679995 The bottom left figure is from: http://pre-xsj.699pic.com/tupian/19368h.html The top right picture is from: https://www.pinterest.com/pin/135882113727321721/https://www.quanjing.com/imginfo/bji05100078.html.

basalt fiber modified 3D printed cement-based materials have not been widely represented. Therefore, further research is needed to enhance the long-term performance and durability of basalt fiber reinforced 3D printing cement-based materials in extreme environments, and data resources in related directions need to be further enriched.

CRediT authorship contribution statement

Canhao Zhao: Writing – review & editing, Writing – original draft. **Xianzhang Guan:** Writing – review & editing. **Xuetao Lyu:** Validation, Supervision. **Ben Li:** Investigation, Funding acquisition, Formal analysis, Data curation, Conceptualization. **Kaihang Li:** Resources, Project administration, Methodology, Investigation.

Declaration of Competing Interest

The authors declare that they have no known competing financial interests or personal relationships that could have appeared to influence the work reported in this manuscript.

Acknowledgement

Thank the colleagues of the ASIM group for their efforts in this work. The authors also thank the Guangdong Fund for Basic and Applied Basic Research (2022A1515110380 and 2022B1515120007), and Heilongjiang Natural Science Foundation Key Project (ZD2022E001).

Data availability

The authors do not have permission to share data.

References

[1] E. Lloret, A.R. Shahab, M. Linus, R.J. Flatt, F. Gramazio, M. Kohler, S. Langenberg, Complex concrete structures: merging existing casting techniques with digital fabrication, Comput. Aided Des. 60 (2015) 40–49.
[2] I. Perkins, M. Skitmore, Three-dimensional printing in the construction industry: a review, Int. J. Constr. Manag. 15 (1) (2015) 1–9.
[3] S.C. Paul, G.P. Van Zijl, M.J. Tan, I. Gibson, A review of 3D concrete printing systems and materials properties: current status and future research prospects, Rapid Prototyp. J. 24 (4) (2018) 784–798.
[4] G.H. Ahmed, N.H. Askandar, G.B. Jumaa, A review of largescale 3DCP: Material characteristics, mix design, printing process, and reinforcement strategies, Structures 43 (2022) 508–532.
[5] Z. Xiaofei, S. Yao, S. Run, L. Shouyi, Experimental study on mechanical properties of RCC with different porosity, Chin. J. Appl. Mech. 40 (4) (2023) 840–847.
[6] M. Amin, I.Y. Hakeem, A.M. Zeyad, B.A. Tayeh, A.M. Maglad, I.S. Agwa, Influence of recycled aggregates and carbon nanofibres on properties of ultra-high-performance concrete under elevated temperatures, Case Stud. Constr. Mater. 16 (2022) e01063.
[7] A.M. Tahwia, G.M. Elgendy, M. Amin, Mechanical properties of affordable and sustainable ultra-high-performance concrete, Case Stud. Constr. Mater. 16 (2022) e01069.
[8] A.M. Tahwia, N. Abdelaziz, M. Samy, M. Amin, Mechanical and light transmittance properties of high-performance translucent concrete, Case Stud. Constr. Mater. 17 (2022) e01260.
[9] I.Y. Hakeem, M. Amin, B.A. Abdelsalam, B.A. Tayeh, F. Althoey, I.S. Agwa, Effects of nano-silica and micro-steel fiber on the engineering properties of ultra-high performance concrete, Struct. Eng. Mech. 82 (2022) 295–312.
[10] A.A. Ghanim, M. Amin, A.M. Zeyad, B.A. Tayeh, I.S. Agwa, Y. Elsakhawy, Effect of polypropylene and glass fiber on properties of lightweight concrete exposed to high temperature, Adv. Concr. Constr. 15 (2023) 179–190.
[11] I.Y. Hakeem, M. Amin, I.S. Agwa, M.H. Abd-Elrahman, O.M. Ibrahim, M. Samy, Ultra-high-performance concrete properties containing rice straw ash and nano eggshell powder, Case Stud. Constr. Mater. 19 (2023) e02291.
[12] I.Y. Hakeem, M. Amin, I.S. Agwa, M.H. Abd-Elrahman, M.F. Abdelmagied, Using a combination of industrial and agricultural wastes to manufacture sustainable ultra-high-performance concrete, Case Stud. Constr. Mater. 19 (2023) e02323.
[13] I.Y. Hakeem, M. Amin, I.S. Agwa, M.S. Rizk, M.F. Abdelmagied, Effect of using sugarcane leaf ash and granite dust as partial replacements for cement on characteristics of ultra-high performance concrete, Case Stud. Constr. Mater. 19 (2023) e02266.
[14] Y. Jacquet, V. Picandet, A. Perrot, Characterization of tensile behavior of fresh cementitious materials, Acids Mater. J. 118 (6) (2021) 217.
[15] W. Haoyi, J. Yaqing, P. Tinghong, Wang Yu, Interlayer bonding property of a 3D printing cementitious material, N. Build. Mater. 46 (12) (2019) 5–8.
[16] L. Zhu, M. Zhang, Y. Zhang, J. Yao, G. Yang, X. Guan, Y. Zhao, Research progress on shrinkage properties of extruded 3D printed cement-based materials, J. Build. Eng. 77 (2023) 107394.
[17] L. He, W.T. Chow, H. Li, Effects of interlayer notch and shear stress on interlayer strength of 3D printed cement paste, Addit. Manuf. 36 (2020) 101390.
[18] Y. Junhong, Y. Zheng, Y. Jiangtou, Y. Kequan, D. Fangyuan, X. Jianzhuang, Research progress on 3D printable fiber reinforced concrete, J. Chin. Ceram. Soc. 11 (2021) 2538–2548.
[19] T. Marchment, J. Sanjayan, Mesh reinforcing method for 3D Concrete Printing, Autom. Constr. 109 (2020) 102992.
[20] A. Ramezani, S. Modaresi, P. Dashti, M.R. GivKashi, F. Moodi, A.A. Ramezanianpour, Effects of different types of fibers on fresh and hardened properties of cement and geopolymer-based 3D printed mixtures: a review, Buildings 13 (4) (2023) 945.
[21] S.A. Khan, S.M. Ghazi, H. Amjad, M. Imran, R.A. Khushnood, Emerging horizons in 3D printed cement-based materials with nanomaterial integration: a review, Constr. Build. Mater. 411 (2024) 134815.
[22] P. de Matos, T. Zat, K. Corazza, E. Fensterseifer, R. Sakata, G. Mohamad, E. Rodríguez, Effect of TiO_2 nanoparticles on the fresh performance of 3d-printed cementitious materials, Materials 15 (11) (2022) 3896.
[23] P. Shakor, J. Sanjayan, A. Nazari, S. Nejadi, Modified 3D printed powder to cement-based material and mechanical properties of cement scaffold used in 3D printing, Constr. Build. Mater. 138 (2017) 398–409.
[24] X. Cao, S. Yu, H. Cui, Z. Li, 3D printing devices and reinforcing techniques for extruded cement-based materials: a review, Buildings 12 (4) (2022) 453.
[25] Y. Ying, L. Ben, X. Liangjun, D. Yuxuan, M. Yaona, X. Yongfei, Research on the influence of basalt fiber on the properties of 3D printed recycled cement-based materials, China Concr. Cem. Prod. 12 (2021) 45–49.
[26] D. Tao, X. Jianzhuang, Z. Shuai, Z. Xinji, Anisotropic behavior in bending of 3D printed concrete reinforced with fibers, Compos. Struct. 254 (2020) 112808.
[27] M.V. Tran, Y.T. Cu, C.V. Le, Rheology and shrinkage of concrete using polypropylene fiber for 3D concrete printing, J. Build. Eng. 44 (2021) 103400.
[28] M. Bohuchval, M. Sonebi, S. Amziane, A. Perrot, Rheological properties of 3D printing concrete containing sisal fibres, Acad. J. Civ. Eng. 37 (2) (2019) 249–255.
[29] G. Ma, Z. Li, L. Wang, F. Wang, J. Sanjayan, Mechanical anisotropy of aligned fiber reinforced composite for extrusion-based 3D printing, Constr. Build. Mater. 202 (2019) 770–783.
[30] F.P. Bos, E. Bosco, T.A. Salet, Ductility of 3D printed concrete reinforced with short straight steel fibers, Virtual Phys. Prototyp. 14 (2) (2019) 160–174.
[31] L. Weihong, W. Qian, C. Xuhao, C. Xidong, C. Yuhong, P. Qiang, Effect of fiber on mechanical properties of 3D printing cement-based materials, J. Exp. Mech. 04 (2021) 499–506.
[32] Zitong Yan, Jun-Jie Zeng, Yan Zhuge, JinJing Liao, Jie-Kai Zhou, Guowei Ma, Compressive behavior of FRP-confined 3D printed ultra-high performance concrete cylinders, J. Build. Eng. 83 (2024) 108304.
[33] M. Hambach, M. Rutzen, D. Volkmer, Properties of 3D-printed fiber-reinforced portland cement paste, 3D Concr. Print. Technol. (2019) 73–113.
[34] C. Wei, X. Sun, Z. Yu, P. Zhang, Experimental study and mechanism analysis on basic mechanical properties of basalt fiber reinforced concrete, Struct. Concr. 24 (2023) 4199–4226.

[35] C. Sheng'ai, X. Xuefeng, Y. Xianjiao, C. Zhao, H. Chengyan, L. Zuolei, Experimental study on the interfacial bond between short cut basalt fiber bundles and cement matrix, Constr. Build. Mater. 256 (2020) 119353.
[36] J.J. Li, Z.M. Zhao, Study on mechanical properties of basalt fiber reinforced concrete, in: Proceedings of the 2016 5th International Conference on Environment, Materials, Chemistry and Power Electronics, pp. 406–410.
[37] A. Mohammed, S. Rafiq, W. Mahmood, R. Noaman, K. Ghafor, W. Qadir, Q. Kadhum, Characterization and modeling the flow behavior and compression strength of the cement paste modified with silica nano-size at different temperature conditions, Constr. Build. Mater. 257 (2020) 119590.
[38] A. Mohammed, S. Rafiq, W. Mahmood, R. Noaman, A.D. Hind, K. Ghafor, W. Qadir, Microstructure characterizations, thermal properties, yield stress, plastic viscosity and compression strength of cement paste modified with nanosilica, J. Mater. Res. Technol. 9 (5) (2020) 10941–10956.
[39] R. Alyousef, B. Ali, A. Mohammed, R. Kurda, H. Alabduljabbar, S. Riaz, Evaluation of mechanical and permeability characteristics of microfiber-reinforced recycled aggregate concrete with different potential waste mineral admixtures, Materials 14 (20) (2021) 5933.
[40] A. Ahmed, P. Abubakr, A.S. Mohammed, Efficient models to evaluate the effect of C3S, C2S, C3A, and C4AF contents on the long-term compressive strength of cement paste, Structures 47 (2023) 1459–1475.
[41] Z.O. Pehlivanlı, İ. Uzun, İ. Demir, Mechanical and microstructural features of autoclaved aerated concrete reinforced with autoclaved polypropylene, carbon, basalt and glass fiber, Constr. Build. Mater. 96 (2015) 428–433.
[42] H. Zhou, B. Jia, H. Huang, Y. Mou, Experimental study on basic mechanical properties of basalt fiber reinforced concrete, Materials 13 (6) (2020) 1362.
[43] Y. Li, J. Zhang, Y. He, G. Huang, J. Li, Z. Niu, B. Gao, A review on durability of basalt fiber reinforced concrete, Compos. Sci. Technol. 225 (2022) 109519.
[44] C. Huimin, X. Chunyan, F. Chao, L. Jing, W. Xiuli, W. Dake, Orthogonal analysis on mechanical properties of basalt–polypropylene fiber mortar. Materials 13 (13) (2020) 2937.
[45] M. Iorio, F. Marra, M.L. Santarelli, J. González-Benito, Reinforcement-matrix interactions and their consequences on the mechanical behavior of basalt fibers-cement composites, Constr. Build. Mater. 309 (22) (2021) 125103.
[46] GB/T50081-2019, Standard for test methods of concrete physical and mechanical properties, China, 2019.
[47] GB 175-2023, Common portland cement, China, 2023.
[48] GB/T 1346-2011, Testmethods for water requirement of normal consistency, setting time and soundness of the portland cement, China, 2011.
[49] SL 42-2010, Technical standard for determination of sediment particle size in open channelsz, China, 2010.
[50] JGJ 52-2006, Standard for quality and inspection method of sand and stone for ordinary concrete, China, 2006.
[51] GB/T 14684-2022, Construction sand, China, 2022.
[52] GB/T 7714-2015, Common portland cement, China, 2015.
[53] HJ 1147-2020, Water quality - Determination of pH - electrode method, China, 2020.
[54] A. Adesina, Performance of cementitious composites reinforced with chopped basalt fibres–an overview, Constr. Build. Mater. 266 (2021) 120970.
[55] V. Fiore, T. Scalici, G. Di Bella, A. Valenza, A review on basalt fibre and its composites, Compos. Part B: Eng. 74 (2015) 74–94.
[56] M. Di Ludovico, A. Prota, G. Manfredi, Structural upgrade using basalt fibers for concrete confinement, J. Compos. Constr. 14 (2010) 541–552.
[57] H. Jamshaid, R. Mishra, A green material from rock: basalt fiber–a review, J. Text. Inst. 107 (2016) 923–937.
[58] V.J. John, B. Dharmar, Influence of basalt fibers on the mechanical behavior of concrete—a review, Struct. Concr. 22 (2021) 491–502.
[59] E. Monaldo, F. Nerilli, G. Vairo, Basalt-based fiber-reinforced materials and structural applications in civil engineering, Compos. Struct. 214 (2019) 246–263.
[60] GB/T 2419-2005, Method for determination of fluidity of cement mortar, China, 2005.
[61] GB/T 17671-1999, Standard for strength testing method of cement mortar, China, 1999.
[62] JGJ/T 70-2009, Standard for test method of basic performance of building mortar, China, 2009.
[63] GB/T 6609. 30-2022, National Technical Committee for Standardization of Plastics (SAC / TC 15) Evaluation method for photoaging properties of plastic polymers Fourier transform infrared spectroscopy and ultraviolet / visible spectroscopy, China, 2023.
[64] GB/T 33502-2017, Specification requirements for recording and reporting of X-ray photoelectron spectroscopy (XPS) data for surface chemical analysis by the National Technical Committee for Standardization of Microbeam Analysis (SAC / TC 38), China, 2017.
[65] GB/T 16594-2008, General rule of scanning electron microscope measurement method for micron length of National Microbeam Analysis Standardization Technical Committee, China, 2008.
[66] GB/T 6609. 30-2022,National Nonferrous Metal Standardization Technical Committee (SAC / TC 243) Alumina Chemical Analysis Method and Physical Properties Determination Method Part 30: Determination of Trace Element Content Wavelength Dispersive X-ray Fluorescence Spectrometry, China, 2022.
[67] L. Weiwei, S. Youjia, A comparative study of two methods in the quantitative analysis of X-ray diffraction phases in sediments, J. Earth's Environ. 8 (01) (2017) 78–87.
[68] U. Atici, Prediction of the strength of mineral-addition concrete using regression analysis, Mag. Concr. Res. 62 (8) (2010) 585–592.
[69] J.S. Chou, C.F. Tsai, Concrete compressive strength analysis using a combined classification and regression technique, Autom. Constr. 24 (2012) 52–60.
[70] Qian Chen Ruoyu, B.O.Soboyejo Alfred, Non-linear and mixed regression models in predicting sustainable concrete strength, Constr. Build. Mater. 170 (2018) 142–152.
[71] R. Arora, Suman, Comparative analysis of classification algorithms on different datasets using WEKA, Int. J. Comput. Appl. 54 (13) (2012) 0975–8887.
[72] ⟨https://www.dw.com/en/is-3d-printing-the-future-for-building-homes/a-58679995⟩.
[73] ⟨http://pre-xsj.699pic.com/tupian/19368h.html⟩.
[74] ⟨https://www.pinterest.com/pin/135882113727321721/⟩.
[75] ⟨https://www.quanjing.com/imginfo/bji05100078.html⟩.